INTERNATIONAL JOURNAL FOR NUMERICAL METHODS IN FLUIDS
*Int. J. Numer. Meth. Fluids* 2004; **46**:533–544 (DOI: 10.1002/fld.775)

# A combined fictitious domain/adaptive meshing method for fluid–structure interaction in heart valves

R. van Loon[1,*,†], P. D. Anderson[2], J. de Hart[3] and F. P. T. Baaijens[1]

[1] *Department of Biomedical Engineering, Eindhoven University of Technology, P.O. Box 513, 5600 MB, Eindhoven, The Netherlands*
[2] *Department of Mechanical Engineering, Eindhoven University of Technology, P.O. Box 513, 5600 MB, Eindhoven, The Netherlands*
[3] *Division of Cardio-thoracic Surgery, University of Amsterdam, P.O. Box 22700, 1100 DE, Amsterdam, The Netherlands*

SUMMARY

A new approach for modelling the fluid–structure interaction of flexible heart valves is proposed. Using a finite element method, a Lagrangian description of a non-linear solid and an Eulerian description of a fluid are coupled by a Lagrange multiplier. This multiplier allows the solid and fluid mesh to be non-conform. Solid displacements and fluid velocities are described well in such a fictitious domain approach. However, the accuracy of pressures and shear stresses in the vicinity of the solid are poor. Therefore an inexpensive mesh-adaptation algorithm is applied, which adapts the fluid mesh to the position of the solid mesh every time step. This minor adjustment of the fluid mesh makes it possible to sustain a physiological pressure gradient across a solid leaflet. Furthermore, shear stresses can be computed at both sides of the leaflet. The method is demonstrated for a 2D example, however with a scope to 3D modelling. Copyright © 2004 John Wiley & Sons, Ltd.

KEY WORDS: fluid–structure; mesh adaptation; fictitious domain; heart valves

## 1. INTRODUCTION

Computational methods can be of great help in understanding heart valve pathologies. The behaviour of the valves (mitral or aortic, mechanical or biological), which should cause no resistence during systole, but need to sustain large pressure gradients during diastole, is however not easy to capture. A variety of models have been proposed throughout the years in order to get better insight in the mechanical behaviour of heart valves. Application of these

*Correspondence to: R. van Loon, Department of Biomedical Engineering, Eindhoven University of Technology, P.O. Box 513, 5600 MB, Eindhoven, The Netherlands.
†E-mail: r.v.loon@tue.nl

Contract/grant sponsor: Hemodyn; contract/grant number: TSGE-1054

Published online 31 August 2004

*Received 9 January 2004*
*Revised 19 June 2004*

models can be distinguished into mechanical heart valve and biological (or polymeric) heart valve analysis.

The stiff mechanical valves will not change shape and hence the valve can be modelled as a rigid body if stresses and strains are not of interest. In an attempt to get information about the flow around a mechanical valve, a canal with rigid walls was considered with a rigid obstacle inhibiting the flow [1]. The angle of the obstacle can then easily be changed. However, the transient behaviour of valve and flow is not captured by such models. An ALE method combined with remeshing as used by Lai *et al.* [2] or a marker method as proposed by Shi *et al.* [3], overcome this problem and capable of capturing transient behaviour.

Compared to the mechanical heart valve, modelling of a flexible heart valve is geometrically and numerically, more complex. The bending stiffness of the leaflets is very low compared to the tensile strength along the leaflet surface. This flexibility results in large geometrical changes of the leaflets when exposed to a pulsatile flow. Despite this flexibility the valve influences the flow greatly since it is attached to the wall and is impermeable. During diastolic phase the valve has to sustain a physiological transvalvular pressure gradient. It is obvious that a numerical code needs to be able to describe all phenomena during a heart cycle.

Compared to mechanical heart valves one is often interested not only in the flow pattern around the leaflets but also the strains and stresses inside the leaflets. A modelling approach was to apply a pressure force onto the leaflets disregarding the fluid [4, 5]. These models show that the interaction between the blood flow and the valve leaflets cannot be neglected. After that, two dimensional models emerged with a two dimensional fluid domain coupled to a solid leaflet. The ALE algorithm is often used as a way of coupling an Eulerian description of the fluid domain to a Lagrangian description of the solid domain. This method is combined with remeshing whenever the quality of the fluid mesh degenerates [6]. Since large rotations of the leaflets within the fluid domain are considered here, this combination of ALE and remeshing is obligatory. When meshes become larger and more complex, computing a new conform mesh, as is required when using an ALE method, can be a difficult and time consuming task.

Another technique for modelling fluid–structure problems, called fictitious domain (FD), was used by Glowinski [7–9] and Bertrand [10]. A Lagrange multiplier is used to couple an Eulerian fluid mesh to rigid solids. This Lagrange multiplier allows the meshes to be non-conform and, more important, no remeshing is necessary. A differentiation of the FD method, in which slender Lagrangian solids are coupled to the Eulerian fluid domain, was introduced by Baaijens [11].

This method was first applied in a two dimensional fluid–leaflet interaction model by De Hart [12]. An extension to 3D was published recently [13, 14]. In these models the compliant solid walls are described using an ALE method while an FD method is used for the leaflets.

However in general, FD methods require an interpolation to the immersed boundary. As a result these methods do not allow for highly accurate descriptions of gradients in velocity field and pressure discontinuities across the immersed boundaries. Hence, in heart valves, where shear and substantial diastolic pressure gradients along the leaflets play an important role in their functioning, the application of FD solely to describe the interaction may not be sufficient.

The goal of this paper is to develop a method that is able to accurately capture stresses along the leaflet boundary. Furthermore, physiological pressure gradients across a leaflet should be computed correctly. The presented method is an extension of the FD method [11, 12], with an inexpensive adaptive meshing technique. By creating an inner fluid curve, that coincides with

 

the solid boundary, only interpolation along (and not across) the boundary is needed, resulting in more accurate solutions. Typical model problems are presented to show the method's ability of describing transvalvular shear stress and pressure discontinuities.

## 2. METHODS

### 2.1. Governing equations

Throughout the whole paper fluid–structure problems are considered in which the fluid is described by the Navier-Stokes equation and the continuity equation,

$$\rho\left(\frac{\mathrm{d}\boldsymbol{v}_f}{\mathrm{d}t}+\boldsymbol{v}_f\cdot\boldsymbol{\nabla}\boldsymbol{v}_f\right)=\boldsymbol{\nabla}\cdot\boldsymbol{\tau}_f-\boldsymbol{\nabla}p_f \tag{1}$$

$$\boldsymbol{\nabla}\cdot\boldsymbol{v}_f=0 \tag{2}$$

in which $\boldsymbol{v}_f$ is the fluid velocity, $\boldsymbol{\nabla}$ the gradient operator, $\rho$ the density and $p_f$ the hydrostatic pressure in the fluid. The viscous part of the Cauchy stress tensor denoted as $\boldsymbol{\tau}_f$ reads,

$$\boldsymbol{\tau}_f=2\eta\boldsymbol{D} \tag{3}$$

in which $\eta$ represents the dynamic viscosity and tensor $\boldsymbol{D}$ the rate of deformation tensor,

$$\boldsymbol{D}=\tfrac{1}{2}(\boldsymbol{\nabla}\boldsymbol{v}_f+(\boldsymbol{\nabla}\boldsymbol{v}_f)^{\mathrm{T}}) \tag{4}$$

An incompressible solid phase is considered, described by

$$\boldsymbol{\nabla}\cdot\boldsymbol{\tau}_s-\boldsymbol{\nabla}p_s=\boldsymbol{0} \tag{5}$$

$$\det(\boldsymbol{F})=1 \tag{6}$$

in which $p_s$ is the hydrostatic pressure in the solid and $\boldsymbol{F}$ the gradient deformation tensor $(\boldsymbol{I}+(\boldsymbol{\nabla}_0\boldsymbol{u}_s)^{\mathrm{T}})$ where $\boldsymbol{u}_s$ is the solid displacement vector and $\boldsymbol{\nabla}_0$ the gradient operator with respect to the reference state. The extra stress tensor $\boldsymbol{\tau}_s$ is defined as

$$\boldsymbol{\tau}_s=G(\boldsymbol{F}\cdot\boldsymbol{F}^{\mathrm{T}}-\boldsymbol{I}) \tag{7}$$

where $G$ is the shear modulus and $\boldsymbol{I}$ the unity tensor.

### 2.2. Coupling

The fluid–structure problems presented throughout this paper consist of a fluid domain ($\Omega_f$) and an immersed solid domain ($\Omega_s$). These two domains are coupled at the boundary ($\partial\Omega_s$) of the solid domain by the constraint, $\boldsymbol{v}_f-\boldsymbol{v}_s=\boldsymbol{0}$. This constraint is applied weakly by introducing a distributed Lagrange multiplier ($\boldsymbol{\lambda}$). The weak forms for Equations (2), (6) and the

 

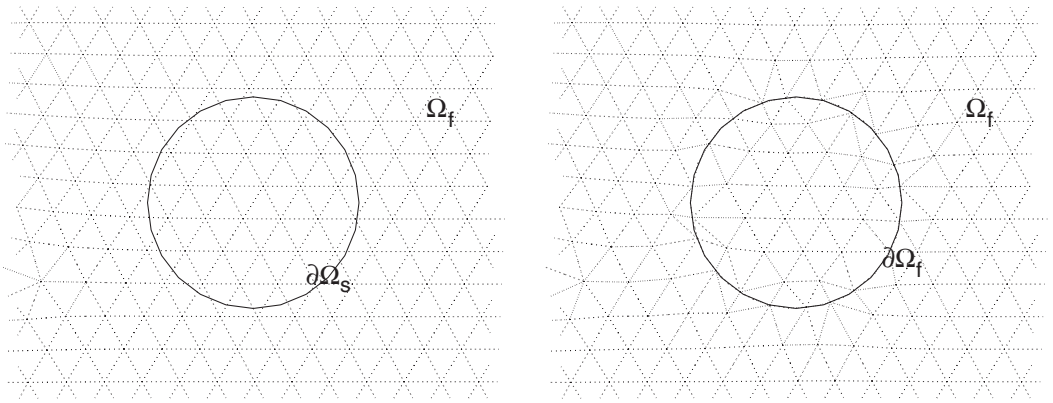


Figure 1. From a solid boundary curve $\partial\Omega_s$ intersecting a fluid domain $\Omega_f$ (a) an inner fluid curve $\partial\Omega_f$ is created, that coincides with $\partial\Omega_s$ (b).

constraint then become,

$$\int_{\Omega_f} \boldsymbol{w}_f \cdot \left( \rho \left( \frac{\mathrm{d}\boldsymbol{v}_f}{\mathrm{d}t} + \boldsymbol{v}_f \cdot \boldsymbol{\nabla}\boldsymbol{v}_f \right) - \boldsymbol{\nabla} \cdot \boldsymbol{\tau}_f + \boldsymbol{\nabla} p \right) \mathrm{d}\Omega_f + \int_{\partial\Omega_s} \boldsymbol{w}_s \cdot \boldsymbol{\lambda}\, \mathrm{d}\partial\Omega_s = \mathbf{0} \tag{8}$$

$$\int_{\Omega_s} \boldsymbol{w}_s \cdot (\boldsymbol{\nabla} \cdot \boldsymbol{\tau}_s - \boldsymbol{\nabla} p)\, \mathrm{d}\Omega_s - \int_{\partial\Omega_s} \boldsymbol{w}_f \cdot \boldsymbol{\lambda}\, \mathrm{d}\partial\Omega_s = \mathbf{0} \tag{9}$$

$$\int_{\partial\Omega_s} \boldsymbol{w}_\lambda \cdot (\boldsymbol{v}_f - \boldsymbol{v}_s)\, \mathrm{d}\partial\Omega_s = \mathbf{0} \tag{10}$$

in which $\boldsymbol{w}_s$, $\boldsymbol{w}_f$ and $\boldsymbol{w}_\lambda$ are appropriate test functions. A same approach is used by Glowinski [8, 9] and de Hart [12] in an FD approach. So far, these methods are generally similar to the one proposed in this paper. The way of applying the Lagrange multiplier is, however, different.

Consider a fluid domain, which is discretized into triangular elements, with a boundary $\partial\Omega_s$ crossing the elements (Figure 1(a)). In the model problems, that de Hart presented, the Lagrange multiplier is defined along the boundary, $\partial\Omega_s$, to couple the velocity of this boundary to the velocity of the fluid elements in which the boundary is situated [12]. Although such an approach gives satisfactory results for valve displacement and the general flow behaviour, it fails to provide an accurate description of shear stresses at either side of the valve. Since boundary $\partial\Omega_s$ crosses the fluid elements, interpolation of the fluid velocity at this boundary results in less accurate solutions. To improve accuracy, mesh refinement is required, which can be expensive if it is not known *a priori* where the solid phase is situated. Furthermore, during diastolic phase of the heart cycle the valves are closed and due to a pressure decrease in the left ventricle, a large pressure gradient occurs across the valve leaflets. Since the leaflets are crossing the fluid elements, erroneous results for the pressures are obtained, which largely influences the velocities.

 

The model proposed in this paper is based on the idea to create a boundary $\partial\Omega_f$ inside the fluid domain that coincides with boundary $\partial\Omega_s$ by performing an adaptation of the mesh in the vicinity of $\partial\Omega_s$ as explained next.

### 2.3. Mesh adaptation

Consider a (fluid) mesh, $\Omega_f$, with an arbitrary solid boundary curve, $\partial\Omega_s$, crossing it as shown in Figure 1(a). In order to create a boundary $\partial\Omega_f$ in the fluid domain that coincides with boundary $\partial\Omega_s$, first the intersections of $\partial\Omega_s$ with $\Omega_f$ need to be found. When all the intersections are determined a selection of fluid nodes, that ensures mesh integrity, are shifted along the intersected curves from the nodes on this curve to boundary $\partial\Omega_s$. The fluid nodes that lie on $\partial\Omega_s$ now form a new inner fluid boundary called $\partial\Omega_f$.

The repositioning of the nodes around the boundary $\partial\Omega_s$ influences the element shapes of this boundary, which can lead to inaccurate results. Therefore, smoothing is applied in this region. The fluid nodes that lie on $\partial\Omega_s$ are not allowed to be shifted. The smoothing can be applied in several node layers around $\partial\Omega_s$ and is based on connectivity. We implemented an algorithm as presented by Freitag [15, 16]. First, one step of Laplacian smoothing is used, in which the new position of a node is calculated by determining the geometrical centre of the surrounding vertex nodes. Second, an angle optimization algorithm is applied in which the angles of elements around $\partial\Omega_s$ are enlarged if they are too small. Per node the surrounding elements and their angles are determined. The node is repositioned such that the smallest of these angles is maximized. Following, in case of second-order extended elements, the midside nodes and centroid are repositioned. The resulting adapted fluid mesh, which can be used for computing, is shown in Figure 1(b).

Now that an inner fluid boundary $\partial\Omega_f$ is obtained that coincides with the solid boundary $\partial\Omega_s$, not only accuracy is gained. It is also possible to take the same discretization for the Lagrange multiplier domain as for $\partial\Omega_f$. From numerical experiments it was found that the weakly coupled system is very sensitive to the amount of coupling elements in which the Lagrange multiplier was discretized and to the order of the interpolation functions of these coupling elements. More or higher-order coupling elements clearly lead to stronger coupling between solid and fluid. However, if the discretization is chosen too fine, the system tends to diverge, as is also observed for interpolation functions of order one and higher. Especially the fluid is very sensitive to the amount of coupling elements. If the discretization of the Lagrange multiplier is based on the solid discretization, it is difficult to control the number of coupling elements within one fluid element. It is therefore convenient to define it based on the discretization of the newly created inner boundary $\partial\Omega_f$.

### 2.4. Solution process

If the combined fictitious domain/adaptive meshing approach is used in time-dependent problems, as will be presented in this paper, the mesh needs to be generated only once. From this mesh, every timestep a second mesh will be created, which is adapted to current solid boundary position. This adapted mesh will be used for computational purposes. The non-linear set of equations is linearized and solved in a Newton–Raphson iterative scheme. Each time step after convergence of this iteration scheme the solid position is updated (an updated Lagrange formulation is used) and a new mesh is created based on the original mesh and the new position of the solid. Following, solutions are mapped from the second mesh onto the newly

 

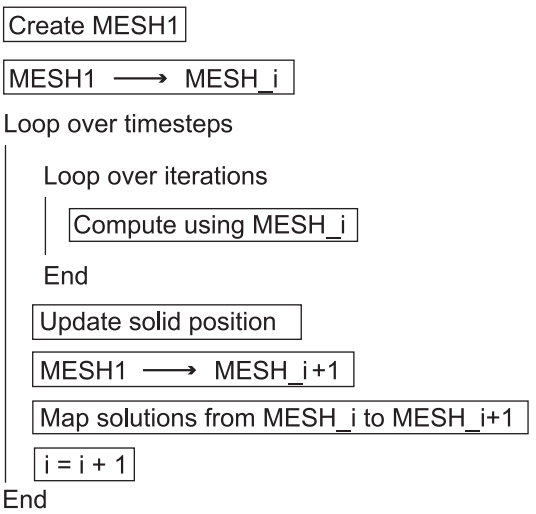


Figure 2. Schematic representation of the program.

created mesh using the basis functions of the fluid elements. A graphical representation of the program is shown in Figure 2. An implicit time-integration scheme is used for both the solid and fluid and a first-order approximation is used for the velocity ($\boldsymbol{v}_f = \boldsymbol{u}_f/\Delta t$ and $\boldsymbol{v}_s = \boldsymbol{u}_s/\Delta t$), where $\Delta t$ is the time step. For the fluid $P_2^+ - P_1$ triangular elements are used and for the solid $Q_2^+ - Q_1$ quadrilateral elements. The Lagrange multiplier domain has the same discretization as the internal fluid boundary that is obtained from mesh adaptation and is integrated using discontinuous linear interpolation functions. Note, that in the model problems, presented in this paper, the thickness and mass of the solid are negligible as far as the interaction with the fluid is considered. Therefore, fluid and solid velocity are coupled at only one boundary of the solid. With respect to the FD method only extra computation time is needed to perform the mesh adaptation and mapping. Since topology does not alter, the adaptation is a relatively small task, especially for large systems. The CPU time needed to perform the mesh adaptation is therefore negligible compared to the time needed for solving the system. The finite element package, SEPRAN [17], is extended for the computations in combination with a direct HSL solver [18].

## 3. RESULTS

In order to show the value of the presented combined fictitious domain/adaptive meshing method in fluid–structure problems with flexible leaflets, two model problems are presented. The first model shows how an applied pulsatile flow will cause a flexible solid slab to deform and move. The flow field in its turn is highly influenced by the slab. As will be highlighted, shear stresses can vary significantly in space and time. The second problem will show the ability of the method to describe a transvalvular pressure drop. To emphasize the necessity of mesh adaptation, a comparison is made with an FD method.

 

### 3.1. *Flexible solid slab in a rigid fluid domain*

An Eulerian fluid domain $\Omega_f$ is considered with an immersed Lagrangian solid domain $\Omega_s$ (Figure 3). Along the walls, denoted with $\Gamma_{\text{wall}}$, a no slip condition applies and at $\Gamma_{\text{inlet}}$ the velocity is prescribed as a function of time,

$$v_f = \sin(2\pi t) \tag{11}$$

over a dimensionless time period of 0.0–1.0. The solid is attached to the upper wall. The fluid is described by the Navier–Stokes equation (2) and the solid by the Neo–Hookean relation (6). As stated earlier the Lagrange multiplier domain is defined along the internal fluid boundary that is obtained from mesh adaptation and coincides with boundary $\partial\Omega_s$. The domain is integrated using linear, discontinuous interpolation functions. To get a stable tip displacement, coupling elements are defined along the solid boundary $\Gamma_{\text{tip}}$, which use constant, discontinuous interpolation functions. For comparison, a fictitious domain computation has been performed using the same mesh. Only, the discretization of the Lagrange multipliers is chosen equal to that of the solid at boundary $\partial\Omega_s$. Constant, discontinuous interpolation functions are used for integration. For all computations concerning this model problem, time is discretized into 4000 time steps. A maximum Reynolds number of 1000 (height of the canal is used as characteristic length) and a maximum Strouhal of 0.1 are used. Large extensions for the inlet and outlet are needed to avoid boundary influences, which leads to a length/height ratio of the canal of 20:1. The fluid mesh is divided into 5004 elements. The solid mesh consists of a length/width ratio of 18:1 and is divided into $20 \times 2$ elements.

Since the tip of the solid can move most freely, its movement is taken as a comparison between both methods. In Figures 4(a), (b) and (c) the tip position is plotted as well as the seperate $x$ and $y$ displacements as a function of time (Note that $x$ is the axial direction). Only small differences are observed in axial direction while a comparison of the methods in $y$-direction shows larger differences. However, although the transient behaviour between maxima and minima is different for both methods, the value and time at which they take place correspond reasonably well. In Figures 5(a), (b) and (c) the solution at $t = 0.575$ is highlighted in a plot of a mesh, a vector plot of the velocity field and a contour plot of the velocity field, respectively. For sake of clarity the long inlet and outlet are not shown in the figures, which leaves the most interesting middle part of the fluid domain to be presented. In this part of the time cycle, the prescribed velocity at the inlet has just changed sign and the solid starts to move from right to left. At this time several vortices are present, which immediately shows the necessity of the extended in and outlet. Time steps have proven to be sufficiently small, as has the element size in the spacial discretization. Computations have

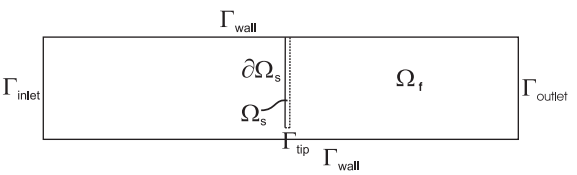


Figure 3. Schematic representation of a flexible slab in a fluid canal.

 

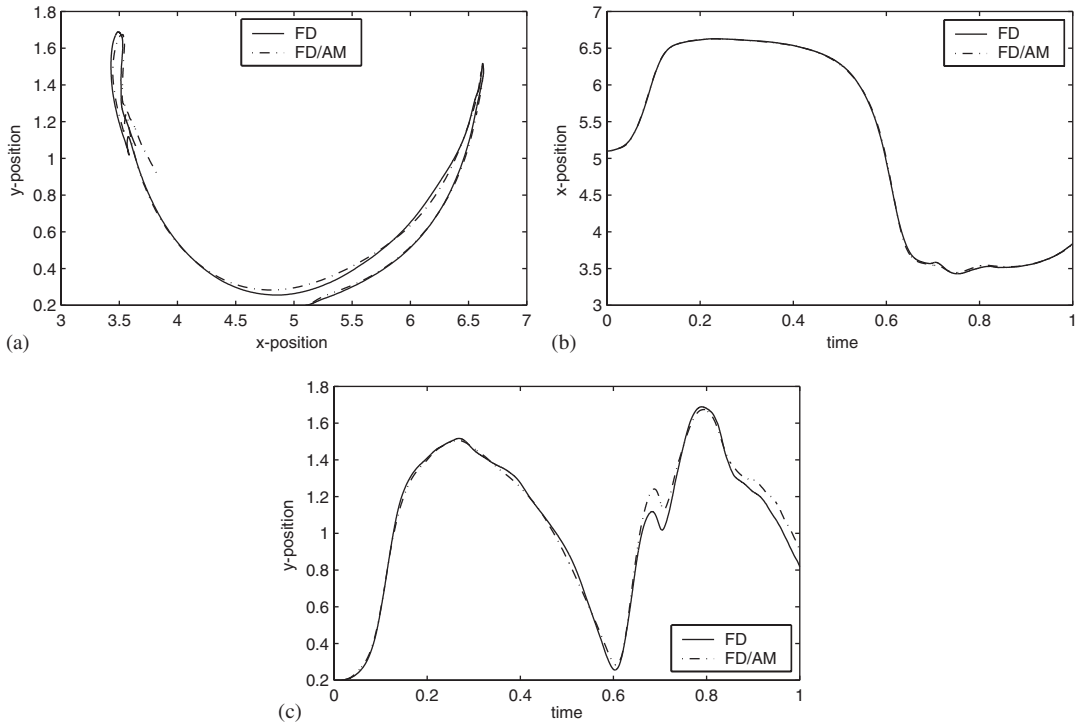


Figure 4. Tip position of the solid during 1 cycle ($t = 0.0 - 1.0$) for the fictitious domain method with (FD/AM) and without (FD) adaptive remeshing (a). Tip position in $x$- and $y$-direction as a function of time shown in (b) and (c), respectively. The fluid mesh consists of 5004 elements and the solid mesh of $2 \times 40$ elements and 4000 timesteps are used.

been performed for different mesh discretizations (1268, 2534, 5004 and 8548 fluid elements) of which the tip displacements are plotted in Figures 6(a), (b) and (c).

As mentioned before, one advantage of the FD method combined with mesh adaptation compared to the FD method without it, is the possibility of gaining information about the shear stresses along the solid. The choice of the $(P_2^+ - P_1)$ elements demands that the computed velocities is continuous across the element boundaries, however, derivatives can be discontinuous. Therefore, it is possible to compute different shear stresses at either side of the solid slab. Figure 7 shows part of the mesh and velocity vector at $t = 0.188$ and Figure 8 shows the corresponding shear stresses along both sides of the solid. The shear stresses in the midside nodes of the fluid element edges along the solid are plotted. Note that since the tip of the solid lies inside a fluid element, no shear stress information at this position is available.

### *3.2. Fluid pressure drop over a flexible solid membrane*

The first model problem incorporated the movement of the valve, the complexity of the flow field and the determination of shear stresses. These are typical phenomena during systole. An important phenomenon during diastole is the moving pressure drop over the leaflets, which is captured in the following model problem. The setup, that is used, is similar to the one shown

 

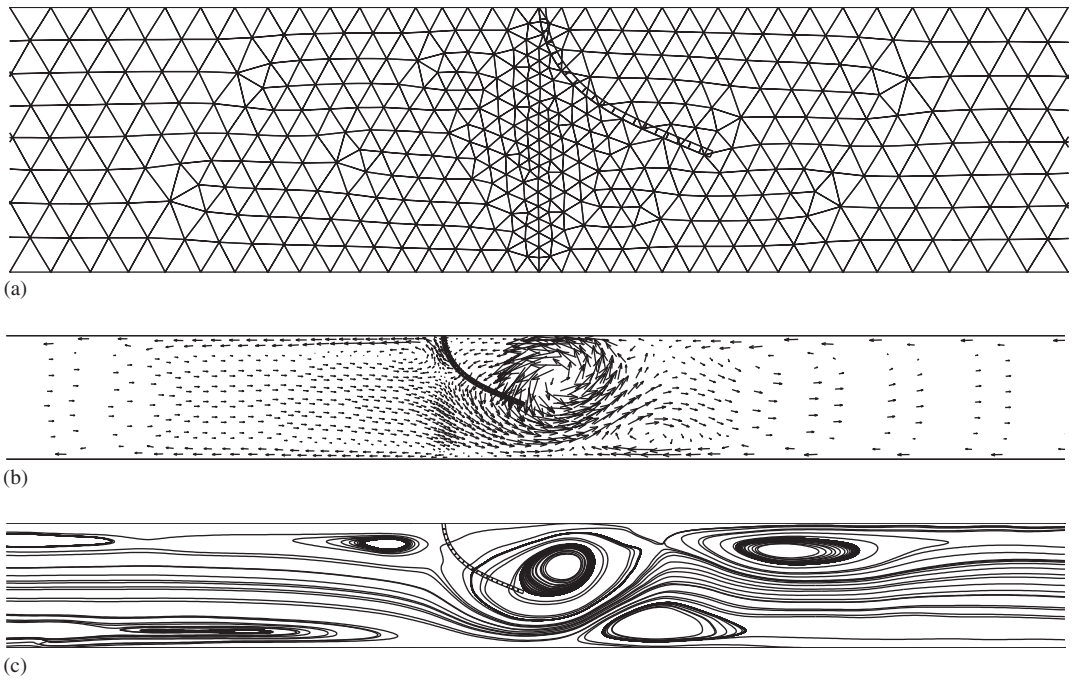


Figure 5. The adapted mesh (a), a vector plot of the velocity field (b) and a streamline plot of the velocity field (c) at $t = 0.575$.

in the former example (Figure 3). The only difference is that solid boundary $\Gamma_{\text{tip}}$ is now connected to the bottom wall with homogeneous Dirichlet boundary conditions. The walls, denoted with $\Gamma_{\text{wall}}$, have homogeneous Dirichlet conditions and at $\Gamma_{\text{inlet}}$ Neumann boundary conditions are prescribed. Coupling between the domains is established at $\partial\Omega_s$. The equations and elements used for fluid and solid are the same as in the former example. Again, the adaptive meshing approach is compared with a fictitious domain approach. As the prescribed pressure builds up the membrane will start to bend and elongate and finally the membrane will find an equilibrium position in which it bears the total pressure. A similar computation is done using FD. However, erroneous results are obtained in the vicinity of the membrane when the pressure jump gets too large (Figure 9(a)). The error in the solution accumulates, which after several time steps leads to divergence of the non-linear system. The FD method combined with adaptive meshing, on the other hand, captures the pressure drop accurately. The $P_2^+ - P_1$ elements are able to describe pressure discontinuities across the element edges. By mesh adaptation an inner fluid curve is created, which enables a drop of the pressure over the valve as would be expected. The corresponding velocity field will not be disturbed by a poor pressure solution in the vicinity of the valve as can be seen in Figure 9(b). First, movement of the valve is induced by the applied pressure as shown in Figure 9(b), but finally the velocity field will be zero with a pressure jump across the membrane.

 

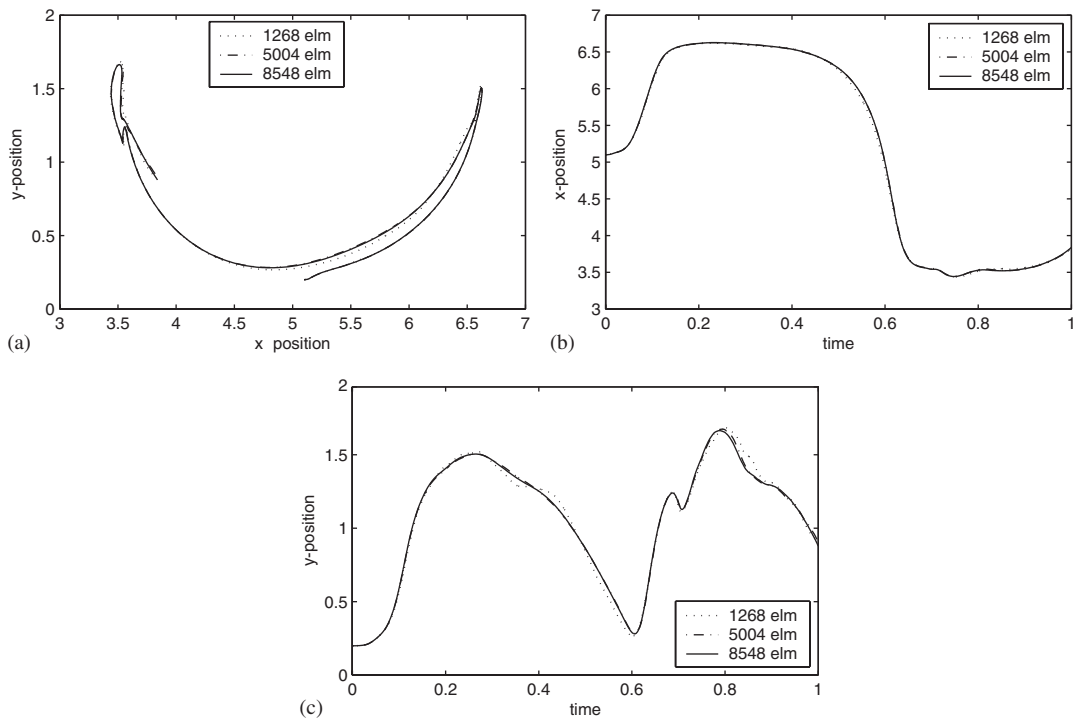


Figure 6. Tip position of the solid during 1 cycle ($t = 0.0 - 1.0$) for different discretizations of the fluid mesh. Tip position in $x$- and $y$-direction as a function of time are shown in (b) and (c), respectively.

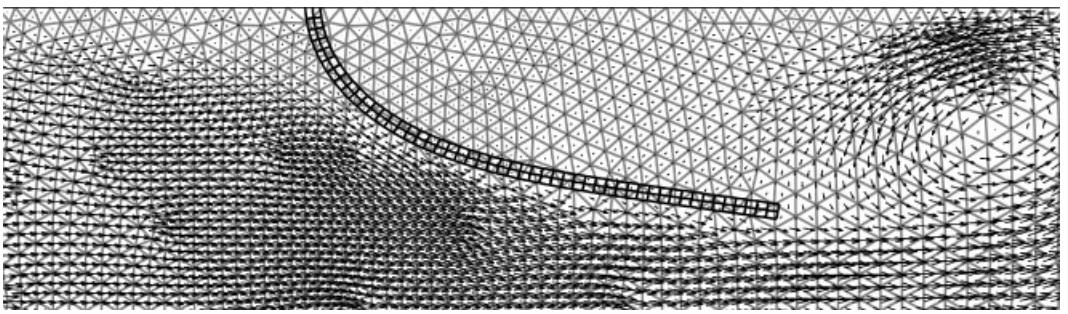

Figure 7. Velocity vector plot on fluid mesh at $t = 0.188$.

## 4. DISCUSSION

A method is presented for modelling fluid–structure problems in flexible heart valves, which is able to accurately capture shear stress along both sides of the leaflets as well as transvalvular pressure gradients. The FD method presented by de Hart [12] is extended with a computationally inexpensive adaptive meshing algorithm. Coupling of a seperate Eulerian and Lagrangian

 

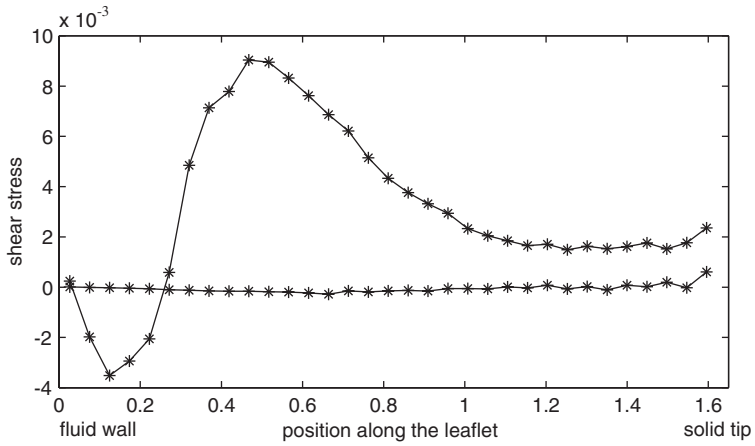


Figure 8. Shear stresses along both sides of the solid at $t = 0.188$.

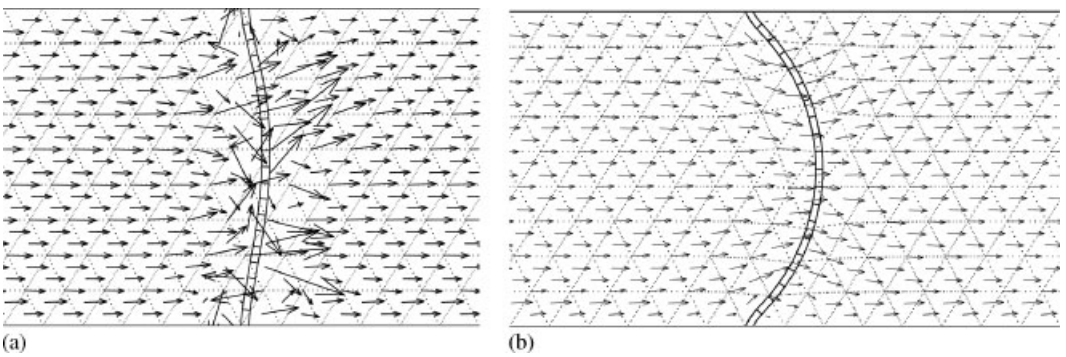


Figure 9. Pressure drop over a membrane using the fictitious domain method with (a) and without (b) mesh adaptation (showing the velocity vector field).

mesh is established using a Lagrange multiplier, which allows for optimal choices of the discretizations of fluid and structure. The coupling between the meshes is enhanced by adapting the Eulerian mesh, such that an inner curve $\partial\Omega_f$ is created which coincides with a solid boundary. Since the fluid mesh is only adapted locally, where the solid crosses fluid elements and since topology remains unchanged, the adaptation algorithm is relatively inexpensive with respect to building and solving the set of equations. The use of a discontinuous pressure discretization in combination with the inner fluid curve $\partial\Omega_f$ enables capturing of the pressure drop across the leaflets. Furthermore, accurate solutions for the shear stress at both sides of the leaflets can be obtained. Two examples are presented in which the method proves to be a significant improvement with respect to the FD method in which the Eulerian mesh is kept unchanged. Since FD methods have proven to be an interesting numerical tool for 3D analysis of fluid–structure problems in heart valves [13, 14], extension of the presented method to three dimensions is a step of great interest. However, in the 3D physiological situation,

 

the three leaflets of the aortic heart valve interact with one another. This solid–solid contact problem was avoided in this paper by considering two separate situations that could be seen as a representation for systole and diastole. In order to describe this transition phase, in which the coaptation areas of the leaflets interconnect, contact algorithms should be incorporated in the computations.

ACKNOWLEDGEMENT

This research is performed in the scope of the Hemodyn project, which is a cooperation between Philips Medical Systems Best, the Technical University Eindhoven and the Erasmus University Rotterdam, the Netherlands. It is financially supported by Senter (Dutch Ministry of Economic Affairs) in their TS subsidy programme (Technologische Samenwerking).

REFERENCES

1. King MJ, David T, Fischer J. Three dimensional study of the effect of two opening angles on the time dependent flow through a bileaflet mechanical heart valve. *Medical Engineering and Physics* 1997; **19**(3):235–241.
2. Lai YG, Krishnan BC, Lemmon J. Numerical simulation of mechanical heart valve closure fluid dynamics. *Journal of Biomechanics* 2002; **35**:881–892.
3. Shi Y, Zhao Y, Yeo TJH, Hwang NHC. Numerical simulation of opening process in a bileaflet mechanical heart valve under pulsatile flow condition. *Journal of Heart Valve Diseases* 2003; **12**(2):245–255.
4. Black MM, Howard IC, Huang X, Patterson EA. A three-dimensional analysis of a bioprosthetic heart valve. *Journal of Biomechanics* 1991; **24**(9):793–801.
5. De Hart J, Cacciola PJG, Peters GWM, Schreurs PJG. A three-dimensional analysis of a fibre-reinforced aortic valve prosthesis. *Journal of Biomechanics* 1998; **31**:629–638.
6. Makhijani VB, Yang HQ, Dionne PJ, Thubrikar MJ. Three-dimensional coupled fluid-structure simulation of pericardial bioprosthetic aortic valve functioning. *ASAIO Journal* 1997; **43**(5):387–392.
7. Glowinski R, Pan TW, Périaux J. A Lagrange multiplier/fictitious domain method for the numerical simulation of incompressible viscous flow around moving rigid bodies: (I) case where the rigid body motions are known a priori. *Comptes Rendus de l' Academie des Sciences Paris* 1997; **25**(5):361–369.
8. Glowinski R, Pan TW, Hesla TI, Joseph DD. A distributed Lagrange multiplier/fictitious domain method for particulate flows. *International Journal of Multiphase Flow* 1999; **324**:755–794.
9. Glowinski R, Pan TW, Hesla TI, Joseph DD, Périaux J. A distributed Lagrange multiplier/fictitious domain method for flows around moving rigid bodies: Application to particulate flow. *International Journal for Numerical Methods in Fluids* 1999; **30**(8):1043–1066.
10. Bertrand F, Tanguy PA, Thibault F. A three-dimensional fictitious domain method for incompressible fluids flow problems. *International Journal for Numerical Methods in Fluids* 1997; **25**(6):719–736.
11. Baaijens FPT. A fictitious domain/mortar element method for fluid-structure interaction. *International Journal for Numerical Methods in Fluids* 2001; **35**(7):743–761.
12. De Hart J, Peters GWM, Schreurs PJG, Baaijens FPT. A two-dimensional fluid-structure interaction model of the aortic value. *Journal of Biomechanics* 2000; **33**(9):1079–1088.
13. De Hart J, Peters GWM, Schreurs PJG, Baaijens FPT. A three-dimensional computational analysis of fluid-structure interaction in the aortic valve. *Journal of Biomechanics* 2003; **36**(1):103–112.
14. De Hart J, Peters GWM, Schreurs PJG, Baaijens FPT. A computational fluid-structure interaction analysis of a fiber-reinforced stentless aortic valve. *Journal of Biomechanics* 2003; **36**(5):699–712.
15. Freitag L, Jones M, Plassmann P. An efficient parallel algorithm for mesh smoothing. In *Proceedings of the Fourth International Meshing Roundtable*, 1995; 743–761.
16. Freitag L, Ollivier-Gooch C. Tetrahedral mesh improvement using swapping and smoothing. *International Journal for Numerical Methods in Engineering* 1997; **40**:3979–4002.
17. Segal G. SEPRAN Introduction. *User's Manual, Programmer's Guide and Standard Problems*, *Ingenieursbureau SEPRA*, Leidschendam, 2003.
18. HSL(2002). A collection of Fortran codes for large scale scientific computation. http://www.numerical.rl.ac.uk/hsl.

 